

Notice

This manuscript is peer-reviewed manuscript that has been accepted and published with in Geophysical Journal International

The manuscript can be cited as follows:

Elías R Heimisson, Jonathan D Smith, Jean-Philippe Avouac, Stephen J Bourne, Coulomb threshold rate-and-state model for fault reactivation: application to induced seismicity at Groningen, *Geophysical Journal International*, Volume 228, Issue 3, March 2022, Pages 2061–2072, <https://doi.org/10.1093/gji/ggab467>

This version submitted to EarthArXiv is the final version of the manuscript, but in a draft format.

Contact: elias.heimisson@sed.ethz.ch

1 Coulomb Threshold Rate-and-State Model for Fault 2 Reactivation: Application to induced seismicity at 3 Groningen

4 Elías R. Heimisson^{1,2*}, Jonathan D. Smith¹, Jean-Philippe Avouac¹, Stephen J. Bourne³

¹ *Division of Geological and Planetary Sciences, California Institute of Technology, Pasadena, 91106, California, USA.*

² *Now at: Swiss Seismological Service, ETH Zurich, Zurich, Switzerland*

³ *Shell Global Solutions, Amsterdam, Netherlands*

5 6 SUMMARY

7 A number of recent modeling studies of induced seismicity have used the rate-and-state
8 friction model of Dieterich (1994) to account for the fact that earthquake nucleation is not
9 instantaneous. Notably, the model assumes a population of seismic sources accelerating
10 towards instability with a distribution of initial slip speeds such that they would produce
11 earthquakes steadily in the absence of any perturbation to the system. This assumption
12 may not be valid in typical intra-plate settings where most examples of induced seismic-
13 ity occur, since these regions have low stressing rates and initially low seismic activity.
14 The goal of this paper is twofold. First, to derive a revised Coulomb rate-and-state model,
15 which takes into account that seismic sources can be initially far from instability. Sec-
16 ond, to apply and test this new model, called the Threshold rate-and-state model, on the
17 induced seismicity of the Groningen gas field in the Netherlands. Stress changes are cal-
18 culated based on a model of reservoir compaction (Smith et al. 2019) since the onset of
19 gas production. We next compare the seismicity predicted by our threshold model and Di-
20 eterich (1994)'s model with the observations. The two models yields comparable spatial
21 distributions of earthquakes in good agreement with the observations. We find however

22 that the Threshold model provides a better fit to the observed time-varying seismicity rate
23 than Dieterich (1994)'s model, and reproduces better the onset, peak, and decline of the
24 observed seismicity rate. We compute the maximum magnitude expected for each model
25 given the Gutenberg-Richter distribution and compare to the observations. We find that
26 the Threshold model both shows better agreement with the observed maximum magni-
27 tude and provides results consistent with lack of observed seismicity prior to 1993. We
28 carry out analysis of the model fit using a Chi-squared reduced statistics and find that
29 the model fit is dramatically improved by smoothing the seismicity rate. We interpret this
30 finding as possibly suggesting an influence of source interactions, or clustering, on a long
31 time-scale of about 3–5 year.

32 **Key words:** Earthquakes; Microseismicity; Seismic-event rates; Earthquake-source mech-
33 anism; b values; Stress distribution

34 1 INTRODUCTION

35 Many prominent examples of anthropogenically induced seismicity occur away from tectonically ac-
36 tive regions in intraplate settings where strain rates and background seismic activity is low. Two well-
37 known examples are the waste-water injection-induced seismicity in Oklahoma (Ellsworth 2013) and
38 the extraction induced seismicity in the Groningen gas field in the Netherlands with, remarkably, no
39 detected historical seismicity (Dost et al. 2017). These two examples, have in common that the onset
40 of induced seismicity occurred at a significant time-lag after the start of injection or production and
41 stress changes in the crust became significant. In Oklahoma the onset of an anomalous seismicity rate
42 occurred about 13 years after injection started (Zhai et al. 2019), but gas was extracted for about 25
43 years from the Groningen gas field before any detected earthquake occurred (Bourne et al. 2014; Smith
44 et al. 2019) (Figure 1a).

45 In order to understand the interplay of injection or extraction and the observed induced seismicity,
46 a number of recent studies have coupled mechanical models of crustal stress changes and the seismicity
47 rate theory of Dieterich (1994) (e.g., Zhai et al. 2019; Candela et al. 2019; Norbeck & Rubinstein 2018;
48 Richter et al. 2020). The theory of Dieterich (1994) is based on empirically derived rate-and-state
49 friction law (e.g. Dieterich 1979; Ruina 1983; Marone 1998). However, in the process of obtaining

* Corresponding author: eheimiss@caltech.edu

50 an attractive expression and maintaining mathematical tractability, several assumptions are made by
51 Dieterich (1994) and further investigated by Heimisson & Segall (2018). A critical assumption is
52 sometimes referred to as the “no-healing limit”, or the “well above steady-state limit”. Dieterich (1994)
53 indeed assumes that some seismic sources in the system must be well above steady-state, meaning
54 that they are accelerating towards instability, regardless of any perturbations to the system. He further
55 assumes that the distribution of their initial state is such that they would result in a steady seismicity
56 rate for a constant background stressing rate. If all the seismic sources are ‘healing’ with time, meaning
57 strengthening due to the evolution of the state variable, then the theory is not strictly valid. We refer
58 the reader to Appendix A for a mathematical definition of the well above steady state limit. Heimisson
59 & Segall (2018) demonstrated a mitigating effect whereby sources initially below steady state can
60 participate in an aftershock sequence (as if they were initially above steady-state) if the step change
61 in stress caused by the main-shock brings the sources above steady state. However, for more gradual
62 stress changes this effect can not be invoked to justify the well above steady-state limit.

63 Regions, such as Oklahoma and Groningen, located in an intra-plate setting with low stressing rates,
64 where induced seismicity only manifests over a decade after start of injection or extraction appear to
65 be in direct contradiction to the well above steady-state limit. As a result, Zhai et al. (2019) found that
66 in order to fit their seismicity rate in Oklahoma they introduced a, somewhat ad hoc, “critical time”,
67 before which stress perturbations to the system are ignored. Candela et al. (2019) used the Dieterich
68 (1994) model for Groningen and obtained an acceptable fit with observed seismicity rate. They, how-
69 ever, had to set initial conditions such that the seismicity rate reached a constant steady-state value
70 only in 1993. While they acknowledge that this is probably an oversimplification, it demonstrates
71 again that the Dieterich (1994) model requires ad hoc modifications in order to be compatible in this
72 kind of an intra-plate setting. Such modifications are typically not needed in more active settings (Stein
73 1999; Jia et al. 2020).

74 Laboratory studies of rocks in both Oklahoma and Groningen would suggest that faults are ca-
75 pable of spontaneously developing seismicity, even in absence of perturbations to the crust. Kolawole
76 et al. (2019) showed that the basement rocks, at conditions appropriate for seismogenic depths, were
77 rate-weakening. Hunfeld et al. (2017) found rate-weakening behavior in Basal Zechstein and a Basal
78 Zechstein and sandstone mixtures, which may affect deeper basement faults. Rate weakening friction
79 is necessary to develop seismic events so the lack of seismicity would suggest that the stress, or the
80 stressing rate, is not sufficient.

81 The idea of a stress threshold in induced seismicity has a long history (Raleigh et al. 1976; Hsieh
82 & Bredehoeft 1981) and in recent modeling studies have introduced various types of thresholds in
83 Oklahoma and Groningen to explain the delayed onset of seismicity. These include critical stress

84 and stress thresholds (Dempsey & Suckale 2017; Dempsey & Riffault 2019), critical injection rate
85 (Langenbruch & Zoback 2016), and critical time (Zhai et al. 2019).

86 Bourne et al. (2018) proposed that the lag in seismicity at Groningen could be explained a prob-
87 abilistic Coulomb failure stress distribution and thus initially the system is generally far from failure,
88 but as continued stressing occurs from extraction more sources are brought to failure. The perspective
89 of Bourne et al. (2018), and continued work by Smith et al. (2021), contrasts that of Candela et al.
90 (2019) by postulating a failure stress distribution and thus a threshold stress for activation, whereas
91 Candela et al. (2019) used the rate-and-state theory of Dieterich (1994) and thus had no threshold
92 stress. These two perspective imply different possible explanation of the lag in seismicity. First, that a
93 stress threshold is needed to initiate failure, the second that a lag in initiation of seismicity is caused
94 by the time-dependence of friction and that the lag could reflect the nucleation time.

95 In this paper we resolve this problem by demonstrating the threshold effect introduced when a
96 population of seismic sources obeying rate-and-state friction and initially far from instability is con-
97 sidered. We apply this threshold rate-and-state model to the Groningen dataset and demonstrate that
98 the model outperforms Dieterich (1994)'s model applied without ad hoc modifications. The paper has
99 three main parts, first we discuss the main features of proposed model and some implications. The
100 model derivation itself is presented in Appendix A and B. Second, we apply the model to the Gronin-
101 gen dataset and compare to the original Dieterich (1994) theory by modeling annual seismicity rates.
102 Finally, we offer a discussion of the broader implications of our findings.

103 **2 THEORY**

104 Here we present the new model, contrast it to the original theory by Dieterich (1994) and discuss some
105 implications. The mathematical derivation is detailed in appendices A and B.

106 In Appendix A we derive an expression for the time to activation of a seismic source, represented
107 by a spring-slider, which is initially well below steady state or healing with time. This initial condition
108 differs from that of Dieterich (1994) who assumes that each source is initially well above steady state,
109 and thus weakening and accelerating towards instability. We find that the time, in which the source is
110 elevated above steady state and begins to weaken, is controlled by a simple stress threshold criterion.

111 In Appendix B, we use the approach of Heimisson & Segall (2018) to derive the seismicity rate
112 for a population of seismic sources that start out initially below steady state and move above steady
113 state with time.

114 Thus in Appendix B we arrive at the following equation:

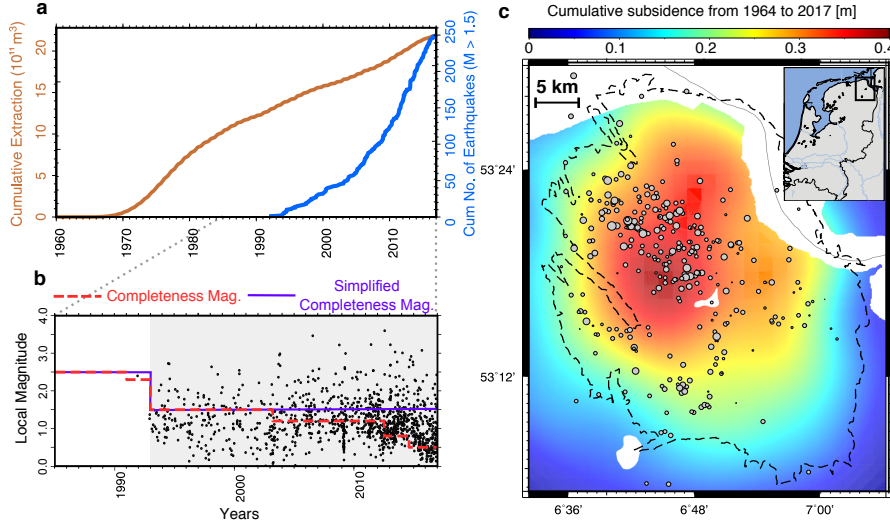


Figure 1. Groningen gas field data overview. a: Cumulative extraction and cumulative number of events with time. Note the large lag between first detected earthquake and the start of production. b: Earthquakes with time along with estimated completeness threshold. In the study we use the more conservative and simplified thresholds, indicated in purple, to filter the catalog. Only seismic observations in the shaded time-period are used to constrain models. We make no assumption about seismicity before 1993. c: Subsidence map used to constrain Coulomb stress model (see Smith et al. 2019; Bourne & Oates 2017)

$$\frac{R}{r} = \frac{\exp\left(\frac{\Delta S(t) - \Delta S_c}{A\sigma_0}\right)}{\frac{1}{t_a} \int_{t_b}^t \exp\left(\frac{\Delta S(t') - \Delta S_c}{A\sigma_0}\right) dt' + 1} \quad \text{if } t \geq t_b$$

$$\frac{R}{r} = 0 \quad \text{if } t < t_b \quad (1)$$

115 where R is the seismicity rate of a population of ‘dormant’ or ‘inactive’ seismic sources at times
 116 $t < t_b$. $\Delta S(t) = \Delta\tau(t) + \mu\Delta\sigma(t)$ is a modified Coulomb stress where the effective coefficient of
 117 friction is $\mu = \tau_0/\sigma_0 - \alpha$ where τ_0 and σ_0 are the initial shear and normal stresses respectively
 118 acting on the population at $t = 0$ and α is the the Linker & Dieterich (1992) constant, which is
 119 generally between 0 and 0.25 and relates changes in normal stress to changes in the frictional state
 120 variable (see equation A.1). ΔS_c is the threshold Coulomb stress. In Appendix A we show that a
 121 seismic source at well-below steady-state will be moved above steady state at a threshold Coulomb
 122 stress that is independent of the stressing history prior to reaching the threshold. The time t_b at which
 123 the threshold stress is reached, is then given by $\Delta S(t = t_b) = \Delta S_c$. We thus stress that t_b is fully
 124 determined by ΔS_c and not an independent parameter. A major difference with the ‘critical time’ of
 125 Zhai et al. (2019) is that if the stressing rate is non uniform then t_b represents a lag that should vary in

space. Finally, as in Dieterich (1994), $A\sigma_0$ is a characteristic stress where A is a constitutive parameter related to the direct effect. $t_a = A\sigma_0/\dot{s}_b$, where \dot{s}_b is the background Coulomb stressing rate, is the characteristic time of aftershock decay following a step increase of stress. Background seismicity rate r is defined as the seismicity rate that the population would reach if elevated above the stress threshold and continuously stressed at \dot{s}_b until ΔS_c is reached. We postulate that ΔS_c could be close to a constant regionally and thus the local onset of seismicity could indicate the stress threshold in areas that have been less perturbed. Thus given a model for the stresses and planned production/injection then one could estimate the time of onset of seismicity, i.e. t_b . However, these ideas need further validation.

Unlike the Dieterich (1994) theory the background rate r is not observable prior to reaching ΔS_c . By definition, if $t < t_b$ and thus the $\Delta S(t) < \Delta S_c$, then $R = 0$ since no seismic sources have been moved above steady state. It is worth highlighting one assumption made in deriving the model (see discussion following equation A.6), which is that stress perturbations should occur on a time-scale much shorter than the time over which the seismic source heals significantly. Thus if \dot{s}_b is very small and no other perturbations occur we cannot expect equation 1 to have an onset of seismicity as at the same stress threshold compared to when large perturbations occur at shorter time-scales.

Following Heimisson & Segall (2018) it is easy to show that the corresponding Dieterich (1994) version of equation 1 is

$$\frac{R}{r} = \frac{\exp\left(\frac{\Delta S(t)}{A\sigma_0}\right)}{\frac{1}{t_a} \int_0^t \exp\left(\frac{\Delta S(t')}{A\sigma_0}\right) dt' + 1}. \quad (2)$$

Comparison of equations 1 and 2 reveals that if $\Delta S_c = 0$ and thus $t_b = 0$ the two equations are the same. We stress that equation 2 is mathematically equivalent, as was shown by Heimisson & Segall (2018), to the Dieterich (1994) model when written with the Coulomb stress approximation of Dieterich et al. (2000):

$$R = \frac{r}{\gamma \dot{s}_b}, \quad \dot{\gamma} = \frac{1}{A\sigma_0} [1 - \gamma \Delta \dot{S}], \quad (3)$$

with γ being a seismicity state variable. Dieterich (1994)'s model is thus a special case of equation 1 in the limit that of no stress threshold.

In order to gain some further insight into equation 1 we derive Omori's law of aftershocks in absence of postseismic reloading. In other words, we explore a special case of a instantaneous jump ΔS in stress at $t=0$. If the $\Delta S > \Delta S_c$ then $t_b = 0$. Then equation 1 gives:

$$\frac{R}{r} = \frac{1}{t/t_a + e^{(\Delta S_c - \Delta S)/A\sigma_0}}, \quad (4)$$

152 which we contrast to the empirical Omori-Utsu law $R = a/(t + c)$, where the decay rate is taken
 153 as $1/t$. As was previously discussed, the corresponding Dieterich (1994) equation is obtain by simply
 154 setting $\Delta S_c = 0$. We thus see that the c parameter in Omori's law depends on ΔS_c . This results in
 155 a lower initial rate of earthquakes in the aftershocks sequence and longer time until the onset of the
 156 characteristic $1/t$ decays than compared to Dieterich (1994) equation.

157 We recognize that if $\Delta S = \Delta S_c$, then $R = r$ and thus no aftershock sequence occurs. This is
 158 consistent with the simulations and analysis of Heimisson & Segall (2018), which show that only
 159 seismic source already above, or elevated above steady state by the coseismic stress step, participate
 160 in the aftershock sequence.

161 3 APPLICATION TO GRONINGEN

162 In this section we compare the threshold rate-and-state model (equation 1) to the original Dieterich
 163 (1994) model (equation 2)

164 3.1 Groningen: Background

165 Gas production at the Groningen gas field, in the northeast of the Netherlands (Figure 1c, inset) began
 166 in 1963 with the most rapid gas extraction in the 70's and a fairly steady extraction rate since 1980
 167 (Figure 1a). In spite of over two decades of extraction and substantial field compaction (Bourne &
 168 Oates 2017; Smith et al. 2019), the first detected earthquake occurred in the 90's (Figure 1a, b). At the
 169 time the seismic network had a magnitude of completeness around 2.3 Dost et al. (2017)(see. Figure
 170 1b), and thus some seismicity may have gone undetected, but in 1993 the seismic network improved
 171 greatly and the completeness magnitude was reduced to 1.5. In the following years, improvements to
 172 the seismic network have further lowered the completeness magnitude. In the following modeling and
 173 analysis, we make the conservative assumption that the completeness magnitude prior to 1993 was 2.5
 174 and 1.5 after 1993 (Figure 1b, purple line).

175 The gas production has caused a substantial compaction of the gas field, which has resulted in sub-
 176 sidence of nearly 0.4 m at its maximum (Figure 1c), and observable seismicity depths ranging from
 177 the reservoir caprock (Smith et al. 2020) to within the reservoir (Willacy et al. 2019; Dost et al. 2017).
 178 Smith et al. (2019) have integrated several different geodetic measurement techniques, used through
 179 time to monitor the compaction of the reservoir. Using a pressure depletion simulation from Neder-
 180 landse Aardolie Maatschappij (2013), they determined the uniaxial compressibility of the reservoir
 181 and found it to be variable in space but pressure-independent (constant in time). Smith et al. (2021)
 182 used the pressure variations and spatially variable compaction of the reservoir to calculate spatial and

183 temporal variations of Coulomb stress. We use the coulomb stress changes from this study to compute
 184 $\Delta S(t)$ in equations (1) and (2). We stress that $\Delta S(t)$ is a function of easting and northing, which we
 185 will denote by x and y respectively. However, all parameters for the purpose of fitting, as is discussed
 186 in the following section, are treated as spatially and temporally constant.

187 3.2 Methods

188 For model comparison we follow strategy of Smith et al. (2021), which is briefly outlined here. Earth-
 189 quakes are placed in yearly bins (Figure 2, red line) following a magnitude filtering for completeness
 190 of 1.5.

191 We quantify misfit using a Gaussian log-likelihood function

$$\log(p(\mathbf{m}|\mathbf{R}^o)) = -\frac{1}{2} \sum_{i=1993}^{i=2016} \left(R_i^o - \int_{\Sigma} R(\mathbf{m}, i, x, y) dx dy \right)^2, \quad (5)$$

192 where $R(\mathbf{m}, i)$ is the model predicted rate density in year i (equation 1 or 2), where \mathbf{m} is the vector of
 193 model parameters. R_i^o is the observed rate in year i . Integration in easting, x , and northing y , is carried
 194 over the area Σ , which is shown by the outlines of the gasfield in Figure 1c. In practice, the integration
 195 is done by splitting the area up in square blocks of 0.25 km². Then take center Coulomb stress in each
 196 block as constant over the area, use the time-history of the Coulomb stress at the location and compute
 197 rate density from equation 1 or 2 assuming that r represents background rate per unit area. Finally
 198 we sum all the blocks. In equation 5 we have assumed that the standard deviation of the observed
 199 seismicity rate is 1 event/year, which is why weighting each term by a variance is omitted in equation
 200 5. Further, the prior probability of the model parameters is uniform and thus only scales the likelihood
 201 function by a constant factor as long as the priors are satisfied. The choice of data standard deviation of
 202 1 is justified only when the rate is estimated by sampling a Poissonian distribution. Then R_i^o represents
 203 the sample mean of the observed rate in each time bin. Because we estimate the seismicity rate by
 204 binning the statistics of the observed rate is not governed by the Poissonian distribution but by the
 205 corresponding sampling distribution of the mean. The expectation value of the sampling distribution
 206 is simply λ where λ is the expectation value of the Poisson distribution and thus $\lambda \approx N$, where
 207 N is the number of events in a fixed time-interval. However the variance of the sample mean is λ/N
 208 and thus the variance is ≈ 1 (see Appendix C for details). Further, we assume sufficiently many events
 209 have occurred in each bin to invoke the central limit theorem such that we can use a Gaussian log-
 210 likelihood function (see also Smith et al. 2021). We acknowledge that for bins with few or no events,
 211 invoking the central limit theorem is not appropriate. However, the Gaussian still serves its intended
 212 purpose of quantifying the goodness of fit and the Gaussian still offers a useful and consistent tool for

the intended purpose of this study, which is the comparison of two models. We stress that the choice of variance model should be considered as minimum variance model and the resulting constraints on model parameters as of the narrowest confidence intervals that can be reasonably obtained. We discuss and provide further justification of this choice in Section 4.2

We use an ensemble Markov Chain Monte Carlo (MCMC) algorithm (Goodman & Weare 2010; Foreman-Mackey et al. 2013) to sample the probability distribution in equation (5) under the constraints of uniform model parameter priors. The uniform priors are placed as follows. r between $6.2 \cdot 10^{-7}$ to $2.5 \cdot 10^{-3}$ events/(year km²). The upper limit is selected as such under that the seismicity in 1993 would correspond to background activity. The lower limit is selected assuming that the field would produce 1 event per 1000 years under background conditions. $A\sigma_0$ is selected between 0.001 to 1 MPa, the range is selected to reflect the typical range from aftershock studies 0.01 to 0.1 MPa (Hainzl et al. 2010), but with considerable additional uncertainty since such values are constrained in very different tectonic settings from the Groningen gas field. t_a has been set between 0.5 years to 10000 years. In aftershock studies this parameter ranges from less than a year to tens of years (Dieterich 1994; Cattania et al. 2014). However, much larger values have been used in induced seismicity modeling. For example Zhai et al. (2019) used $t_a = 6600$ year as their reference model for Oklahoma. We thus choose a prior to reflect this large range of values used elsewhere. However, we acknowledge that our yearly average treatments of seismicity rates would likely prevent us from resolving small values of t_a and the finite time of the observation period should also prevent resolving very large values of t_a . See further discussion in the next section.

3.3 Results

Comparison of the MCMC sampling are shown in Figure 2 where results using equation 1 and 2 that is the new Threshold model and the original Dieterich (1994) model. We have highlighted the *maximum a posteriori* or MAP model in blue, which here maximizes the likelihood function and satisfies the priors. Comparison of the data and the MAP reveals that the threshold model shows considerably better agreement from 1993 – 2003, where the Dieterich (1994) model overpredicts the rate systematically. Further from 2014-2017 a decline in the rate is observed in the data and the threshold model prediction, but not in the Dieterich (1994) model. The model of Candela et al. (2019) similarly fails to match the observed decline. Another striking difference occurs prior to 1993 and thus before the time range used to constrain the model. The threshold model suggests both later onset of seismicity and lower seismicity rate prior to the increased network sensitivity in 1993.

While a qualitative comparison by eye strongly suggests that the fit to the Threshold model is significantly better than the original Dieterich (1994) (see Figure 2) it is worth testing quantitatively

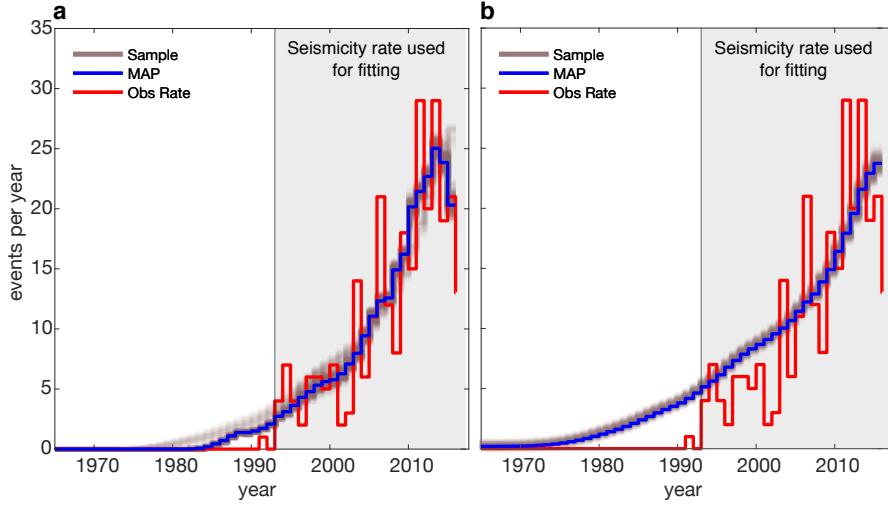


Figure 2. Time series fitting to seismicity rate where a is the threshold model and b is the Dieterich model. The seismicity rate before 1993 (outside gray box area) is not used in fitting. Red line is observed yearly rate filtered by the simplified completeness. Brown are plausible sampled models, blue line is the preferred model. Notice a much earlier onset of seismicity for the Dieterich model and that the model doesn't capture the decrease in the rate at the end of the time-series. We note that the drop in rate (red line) at the end of the time-series represents a further reduction in seismicity rate in the next year of 2017. However, this is beyond the time-scale of the stress model and not included in the modeled rate (e.g. blue).

246 if the model fit is better given that the additional degree of freedom added by introduction of ΔS_c .
 247 Since the Dieterich (1994) model is fully nested in the new Threshold model (a limiting case where
 248 $\Delta S_c = 0$), a simple F-test is appropriate for model comparison (Menke 2018). Using the MAP model
 249 (Figure 2), in both cases to compute the residual sum of squares the F-test indicates that the null
 250 hypothesis, which stated that the improvement in fit can be exemplified by random fluctuations, can be
 251 rejected with a $p = 0.015$. This therefore suggests that the improvement in fit is very likely significant.

Table 1. List of MCMC sampling results rounded to two significant digits

Model	Parameter	95% conf. interval	MAP value	prior range	unit
Threshold	r	$4.0 \cdot 10^{-6} - 3.2 \cdot 10^{-4}$	$5.0 \cdot 10^{-6}$	$6.3 \cdot 10^{-7} - 2.5 \cdot 10^{-3}$	events/(year·km ²)
Dieterich	r	$6.3 \cdot 10^{-5} - 1.3 \cdot 10^{-4}$	$1.0 \cdot 10^{-4}$	$6.3 \cdot 10^{-7} - 2.5 \cdot 10^{-3}$	events/(year·km ²)
Threshold	$A\sigma_0$	0.0046 – 0.040	0.006	0.001 – 1	MPa
Dieterich	$A\sigma_0$	0.041 – 0.050	0.045	0.001 – 1	MPa
Threshold	t_a	720 – 9800	8700	0.5 – 10000	years
Dieterich	t_a	9000 – 10000	10000	0.5 – 10000	years
Threshold	ΔS_c	0.07 – 0.18	0.17	0 – 0.5	MPa

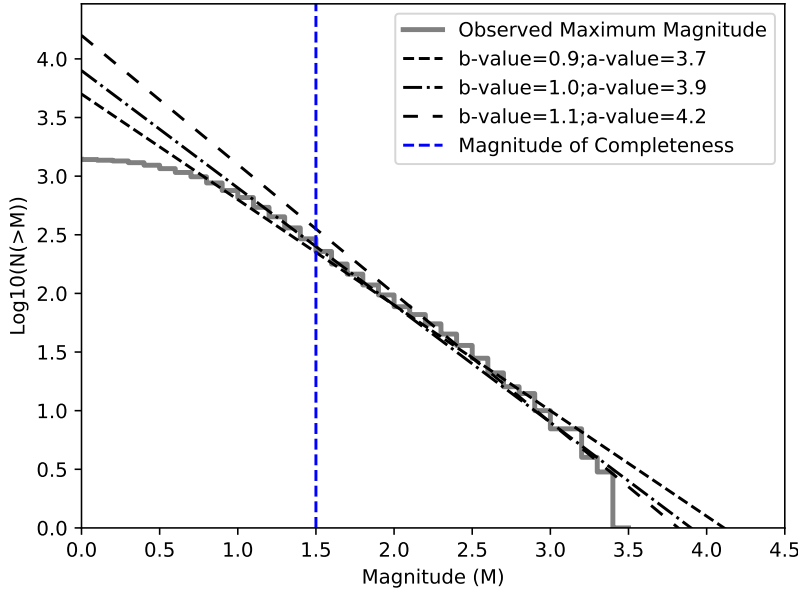


Figure 3. Magnitude-frequency distribution of earthquakes within the Groningen Gas field reported by KNMI (Koninklijk Nederlands Meteorologisch Instituut, <http://www.knmi.nl/>) between 1991 and 2016 . $N(>M)$ is number of earthquakes with magnitude larger than M . The vertical dashed blue line shows the estimated magnitude of completeness. We also show for reference the theoretical Gutenberg-Richter laws obtained for the most likely b -value ($b=1.0$) and the values bounding the 95% confidence range ($b=0.88$ – 1.12) determined by Bourne & Oates (2020).

252 The MCMC sampling provides constraints on model parameters. Based on 1 million samples for
 253 both models, the following 95% confidence intervals are in Table 1. We stress, as was previously men-
 254 tioned, that the confidence intervals are derived under the assumption of a small data variance and no
 255 additional sources of uncertainty and thus the parameter bounds may be smaller than for other ap-
 256 proaches. Nevertheless the analysis reveals large uncertainty on some parameters and the intersection
 257 of confidence bounds for the two models implies strongly that they are in agreement.

258 First, we observe in Table 1 that the confidence bounds on the background rate r of the two model,
 259 threshold and Dieterich (1994) intersects although the MAP values are quite different. However, the
 260 bounds on $A\sigma_0$ for the two models do not overlap, and the Threshold model is better fit with smaller
 261 value of $A\sigma_0$ than the Dieterich (1994) model. Most striking difference in the parameter estimates is
 262 seen in t_a . The threshold model doesn't place much constraint on t_a since the confidence interval is
 263 nearly the prior range. Nevertheless, it is notable that small values ($t \lesssim 500$ years) are rejected and
 264 thus indicating that typical values for active tectonic settings are not appropriate. The Dieterich (1994)
 265 model favors t_a as large as possible and the samples cluster at the prior boundary at 10000 years. We

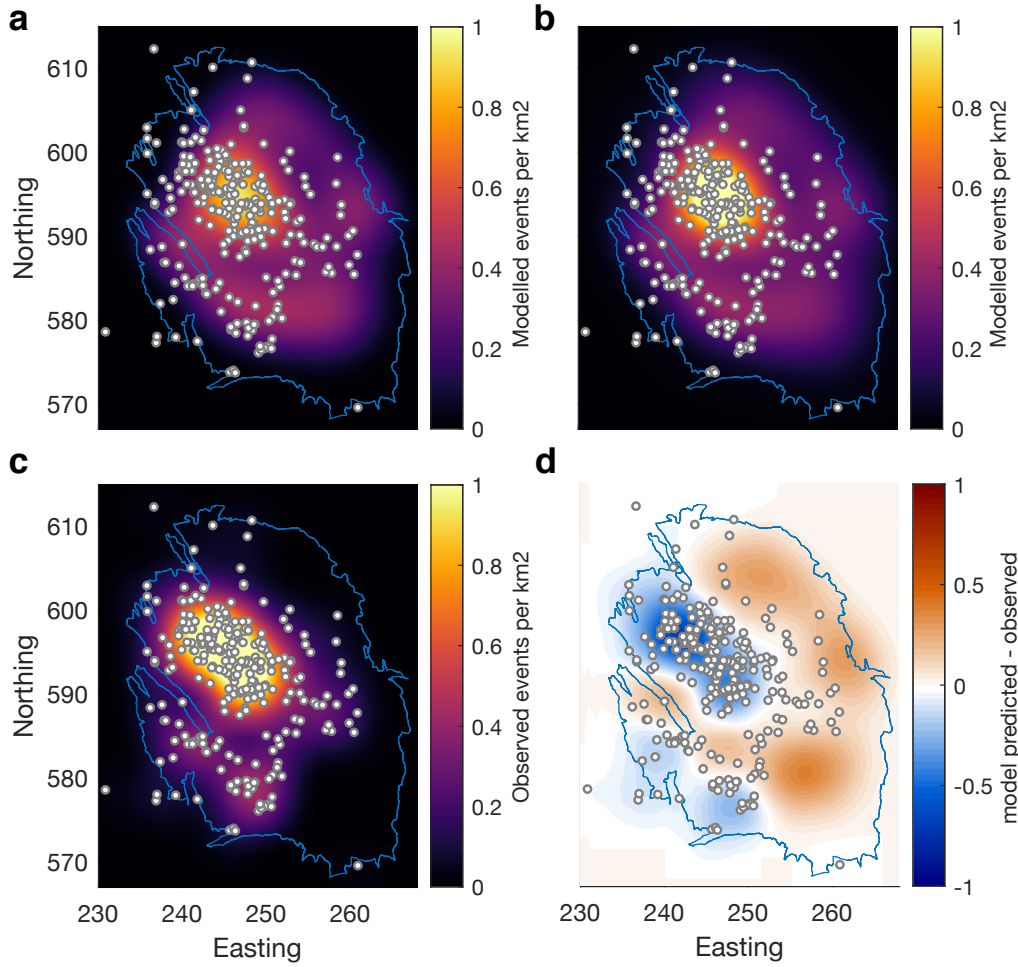


Figure 4. Spatial distribution of events in 2017. a: Model prediction of earthquake density by the threshold model with events plotted on top for references. b: Model prediction by the Dieterich model. c: Observed density with the same resolution as the model. d: Difference between observed density and threshold model density.

266 tested expanding the prior further but found an only slightly improved fit. We discuss the implications
 267 of the t_a estimate further in Section 4.1. Finally we obtained an value ΔS_c from the threshold model,
 268 but we highlight that if $\Delta S_c = 0$ then the Threshold model reduces to the Dieterich (1994) model.
 269 Thus another way to interpret the Dieterich values in Table 1 is that they represent the parameter
 270 estimate if ΔS_c is forced to be at the lower limit of the prior. Clearly the lower bound on acceptable
 271 ΔS_c is 0.07 MPa, which forces systematic differences in the two models and improves the fit for the
 272 Threshold model.

273 All spatial constraints for the seismicity rate come from the Coulomb stress field $\Delta S(t, x, y)$ re-
 274 ported by (Smith et al. 2021) and equation 5 doesn't explicitly penalize models depending on local
 275 spatial agreement such as a space-time Poissonian log-likelihood would (Ogata 1998). Nevertheless

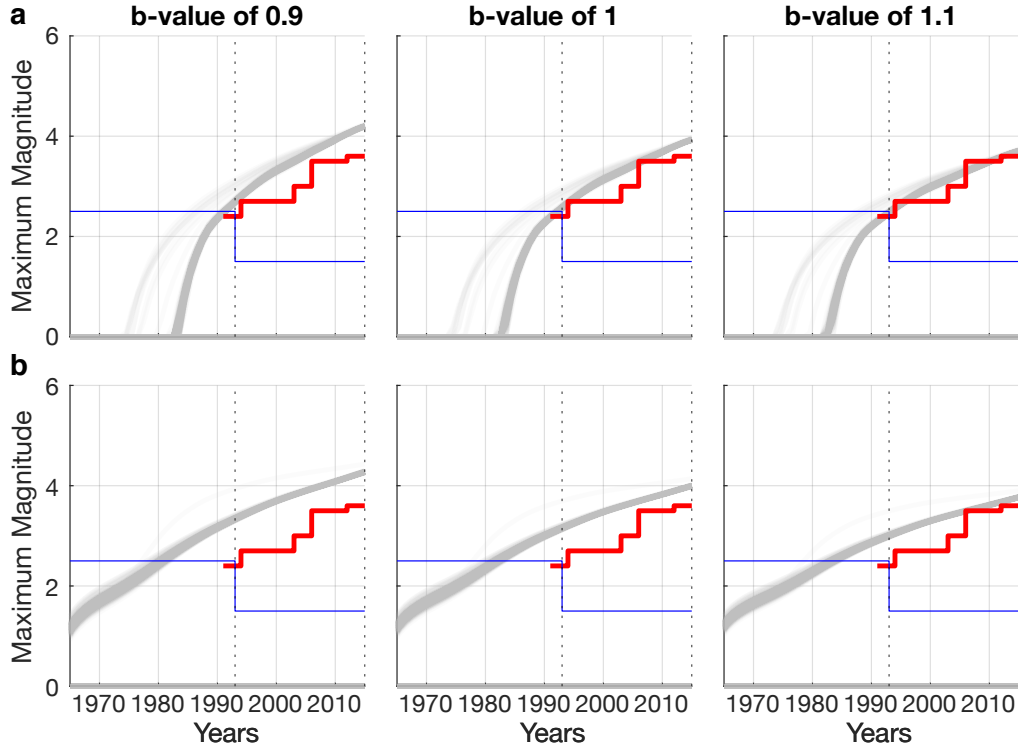


Figure 5. Analysis of model predicted maximum magnitude with time given a Gutenberg-Richter distribution. Gray lines are sampled probable models realizations given a b-value on top of each column. Red is the observed maximum magnitude. Blue is the simplified completeness magnitude. a (top row) uses the Threshold model. Notice that gray lines exceed completeness threshold about the same time as observed seismicity b (bottom row) uses the Dieterich model. Notice that the gray lines are well above the completeness threshold before any detected seismicity occurs.

276 comparing the Threshold model (Figure 4a) and Dieterich (1994) model (Figure 4b) and the observed
 277 rate (Figure 4c) when the earthquake spatial distribution is filtered to the same length-scale of 3 km,
 278 which is the minimum resolvable length scale in the Coulomb stress formulations. We find both the
 279 Threshold model and Dieterich (1994) model to be in a reasonable agreement with the spatial distribu-
 280 tion where in both cases the correlation of earthquake density in each block compared to the observed
 281 slightly exceeds 0.75. However, clear deficiencies are observed, in particular in the southeast of the
 282 gas field where the models over-predict the seismicity rate.

283 To better assess if the Threshold model or the Dieterich (1994) model are in better agreement with
 284 the lack of observed seismicity prior to 1993, we compute the expected maximum magnitude (Van der
 285 Elst et al. 2016):

$$M_{max} = M_c + \frac{1}{b} \log_{10}(N), \quad (6)$$

286 where b is the b-value of the Gutenberg-Richter distribution, which we have plotted and estimated
 287 for the catalog in Figure 3. M_c is the magnitude of completeness, N is the total cumulative number
 288 of events as predicted by integrating equation 1 or 2. Comparison of the two models to the observed
 289 maximum magnitude with time and the simplified completeness magnitude reveals (Figure 5) that
 290 for typical b-values the Threshold model is consistent with the lack of observed prior seismicity and
 291 shows good agreement with the observed maximum magnitude for b-value 1 and 1.1. As seen in
 292 Figure 3, these values are in good agreement with the catalog used. However, the Dieterich (1994)
 293 model (Figure 5b) would suggest that magnitudes large enough to be detected should have occurred
 294 much earlier, furthermore, the agreement with observed maximum magnitude is poor for the explored
 295 b-values in Figure 5.

296 An independent determination of the b-value when the whole catalog is used was found to be
 297 around 1 ± 0.12 assuming no stress dependence of the b-value (Bourne & Oates 2020). We emphasize
 298 that the analysis in this section is based on the assumption that the b value is constant in time and
 299 space, but some evidence suggests that this may not be the case (Bourne et al. 2014; Bourne & Oates
 300 2020).

301 **4 DISCUSSION**

302 **4.1 Parameter estimates**

303 The most striking disparity in parameters estimates between the Threshold model and the Dieterich
 304 (1994) models is in the characteristic decay time t_a . The Dieterich (1994) model estimates this param-
 305 eter to be very large and, in fact, the estimate is limited by the prior upper range at 10000 years (see
 306 Table 1). The Threshold model, on the other hand, does not place much constrain on the parameter.

307 The estimate of t_a is critical to forecast the seismicity in response to any change of the production
 308 rate, in particular, once production ends. t_a represents the time it takes the system to return to back-
 309 ground seismicity rate following a stress step. Thus a large t_a means a sustained seismic hazard for a
 310 long time. A short t_a represents a rapid decline of seismic hazard. However, it is worth noting that in
 311 presence of deformation processes that would relax the imparted stresses then t_a would over-estimate
 312 the duration of sustained seismic hazard level.

313 To investigate further the differences in the two models following a shut-in of production, we
 314 consider a scenario where in 2017 all production ceased. We assume after shut-in the perturbations in
 315 the stress field are spatially and temporally constant. This is not rigorously the prediction for a shut-
 316 in in 2017 as the non-uniform pressure in the reservoir at the time of shut-in would imply be some
 317 small stress variations after shut in. It is, however, probably a close approximation that doesn't require

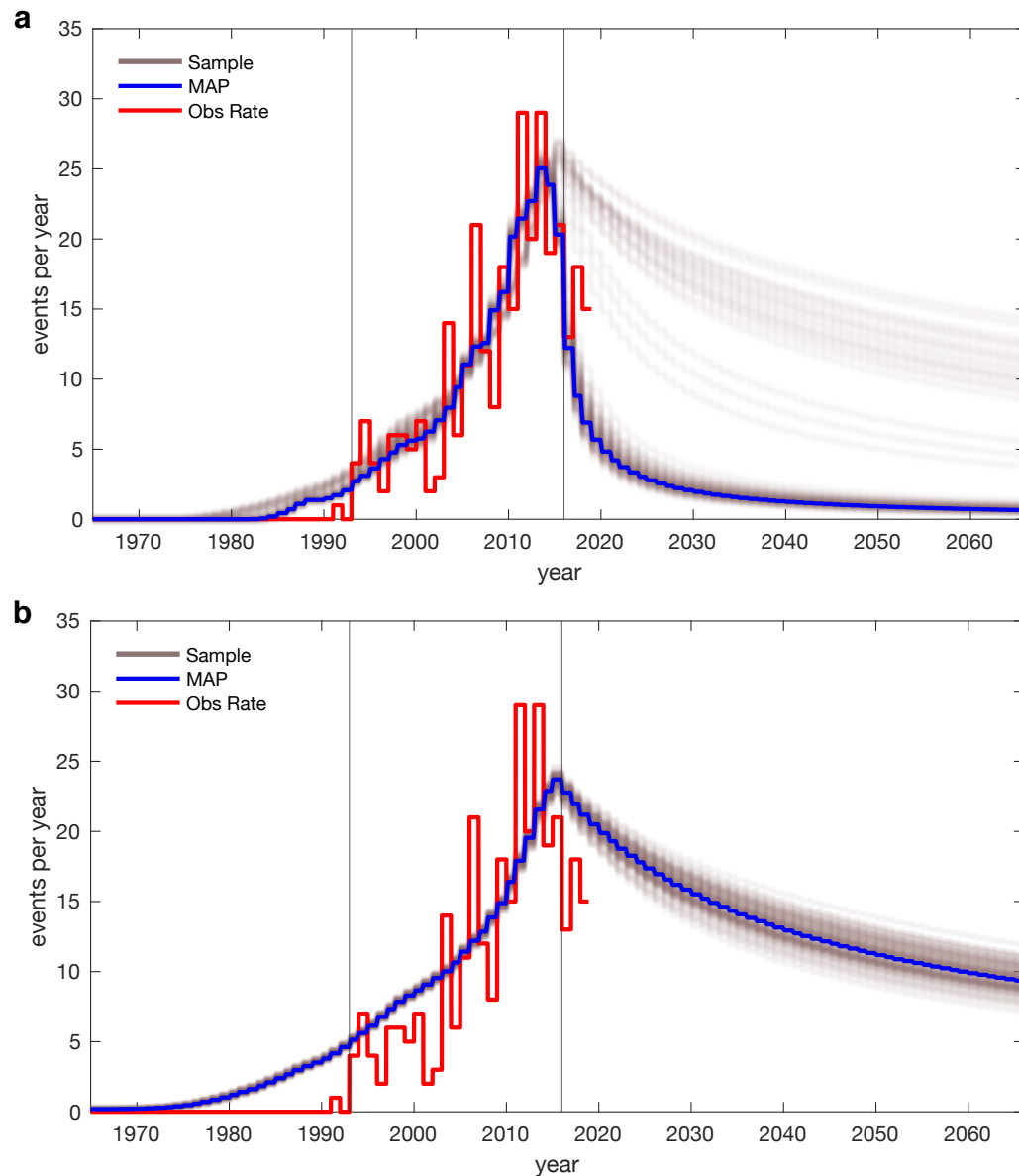


Figure 6. Seismicity rate for the Threshold model (a) and Dieterich (1994)'s model (b) after an abrupt hypothetical stop in production (shut-in) in 2017. The two vertical lines indicate the time-period used for model fitting and sampling. The Threshold model shows considerable variability following a shut-in, but most models show a fairly rapid decay of the seismicity rate, including the favored MAP model. However, all samples for the Dieterich (1994) model indicate a fairly slow decay of the seismicity rate and suggest a substantially elevated seismic risks for several decades after shut-in

318 reservoir modeling and is sufficient to illustrate how the forecast differs if a threshold is introduced in
 319 the Dieterich (1994) model.

320 Figure 6 demonstrates clearly the differences in the two models. The Threshold model shows
 321 some variability in how the seismicity rate decays, however, most realizations cluster around the MAP

322 model that indicates rapid decay of the seismicity rate in the decades following shut-in. The variability
 323 is most likely explained by the fact that t_a is not well constrained by the optimization period, but the
 324 hypothetical scenario presented indicates that a shut-in procedure would place considerable constraints
 325 on the t_a parameter in the next few years after shut-in.

326 Much less variability is observed after shut-in from Dieterich (1994)'s model (Figure 6b), further-
 327 more, all realizations suggest a substantially elevated seismicity for several decades after the shut-in.
 328 Thus applying the Dieterich (1994) model to the Groningen dataset implies that increased seismicity
 329 rate may be observed for very long time following a stop in production at Groningen, however, the
 330 threshold model suggests that t_a can't be well determined with the available data, but could be much
 331 smaller than suggested by the application of the model of Dieterich (1994). In summary, it is evi-
 332 dent that if these model are used to perform a seismic hazard analysis for various end-of-production
 333 scenarios they would render significantly different results.

334 Another critical difference of the parameter estimates manifests in that the Dieterich (1994) model
 335 represents a limiting case of the Threshold model where the threshold $\Delta S_c = 0$. It is worth highlight-
 336 ing that all parameters are assumed spatially constant, including ΔS_c but the stress field $\Delta S(t', x, y)$
 337 is not (Smith et al. 2021). Thus the threshold is reached at different times in different places. Firstly,
 338 this distinguishes the model from the critical time model of Zhai et al. (2019) where the critical time
 339 represented a regional activation of seismicity regardless of local stress state. Secondly, estimating
 340 ΔS_c may have predictive value for activation of seismicity in areas of small stress as production or
 341 injection continues.

342 **4.2 Unmodeled variance**

343 For further analyzing the discrepancy in model and data we compute a χ_ν^2 value, that is chi-squared
 344 reduced value, (e.g. Menke 2018)

$$\chi_\nu^2 = \frac{1}{\nu} \sum_{i=1993}^{i=2016} \left(R_y^o - \int_{\Sigma} R(\mathbf{m}, i, x, y) dx dy \right)^2, \quad (7)$$

345 where ν is the degrees of freedom ($\nu = 19$ for the Threshold model, $\nu = 20$ for the Dieterich (1994)
 346 model) and we have taken the variance as 1 (see Appendix C for explanation). χ_ν^2 value significantly
 347 larger than 1 indicates a poor fit, or an underestimation of the variance. χ_ν^2 value significantly less
 348 than 1 indicates usually over fitting. Thus a $\chi_\nu^2 \approx 1$ is indicative of a fit that is in agreement with the
 349 variance.

350 Using the MAP model (Figure 2) and the observed rate we obtain $\chi_\nu^2 = 19.3$ for the Threshold

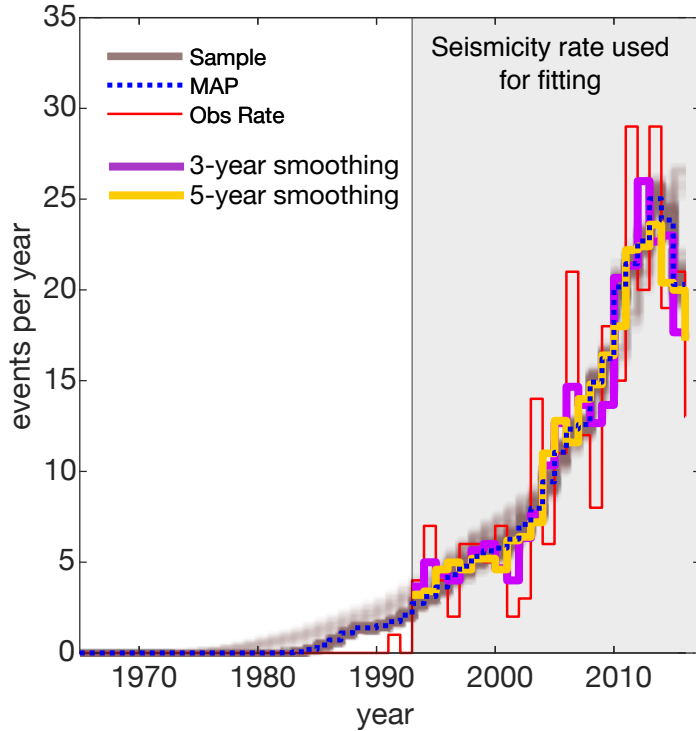


Figure 7. A modification of Figure 2a where we have added 3 and 5 year running average smoothing of the observed rate. This reveals a remarkably good agreement between the MAP model (dashed blue), which represents that optimal model constrained on the data in red given the priors, and the 5 year smooth (yellow)

351 model and $\chi^2_{\nu} = 25.3$ for the Dieterich (1994) model. Although the Threshold model performs better,
 352 the large value of χ^2_{ν} indicates that the variance is severely underestimated.

353 However, we observe that model appears to average the various fluctuations in the observed rate
 354 with time. Thus we test computing χ^2_{ν} after 3 and 5 year running mean smoothing (Figure 7) using the
 355 same model as before (constrained by the red line data). We obtain $\chi^2_{\nu} = 2.77$ and 1.36 for 3 and 5 year
 356 smoothing respectively (Figure 7, purple and yellow) for the Threshold model. We find $\chi^2_{\nu} = 8.94$ and
 357 6.07 for 3 and 5 year smoothing respectively for the Dieterich (1994) model (not plotted). This implies
 358 a close to ideal χ^2_{ν} value for 5-year smoothing if the Threshold model is used and some improvement
 359 for the Dieterich (1994) model although still significantly larger than 1.

360 We suggest two interpretations of this result that need further investigation. Firstly, the averaging
 361 by a running mean may be compensating for temporal earthquake-earthquake clustering occurring on
 362 a long time scale of about 3–5 years. This would be in agreement with the interacting rate-and-state
 363 model of Heimisson (2019) where interactions were not found to change the average number of
 364 events on long time-scales. This finding may also be in agreement with recent results of Post et al.
 365 (2021) that suggested that about 27% of the Groningen catalog may be earthquake-earthquake trig-

366 gered events. Secondly, the variance model used in this study is reasonably justified, from an obser-
367 vational point of view, if the goal is not to model short term variations in the seismicity rate.

368 **4.3 Poissonian log-likelihood**

369 It is a more common practice to carry out optimization and model comparison of seismicity rate models
370 using a Poissonian log-likelihood (e.g. Ogata 1998) model rather than a Gaussian log-likelihood as has
371 been done here. It is thus worth discussion the rationale for our choice.

372 The choice of a Poissonian log-likelihood is motivated by two main reasons. Firstly, that earth-
373 quake rates are count rates and thus negative values are non-physical. Second, that studies have shown
374 that earthquakes are Poissonian point processes (e.g. Gardner & Knopoff 1974). However, the latter
375 property is contingent on removing temporal clustering, or aftershocks, which cause temporal corre-
376 lation in the rate and violate the Markov property of a Poissonian process. The declustering process is
377 nonunique where different algorithms, intended for the same purpose, can render different results (e.g.
378 Marsan & Lengline 2008; Mizrahi et al. 2021). Declustering is particularly problematic for induced
379 seismicity where the external forcing imposes spatial and temporal correlation of events superimposed
380 on aftershock correlation. Declustering in these cases has been found to lead to counter-intuitive deci-
381 sion making and results (Maurer et al. 2020).

382 However, the principal reason we do not use a Poissonian log-likelihood function in this study is
383 that the threshold model will take a value of $R = 0$ before the threshold is reached. This means that
384 Poissonian log-likelihood function assigns exactly 0 probability to models where an event is observed
385 but the theoretical rate is zero ($R = 0$). We tested using a Poissonian log-likelihood from Ogata
386 (1998) for sampling, but found this property to lead to restrictive sampling and poor fit. Considering
387 all the uncertainty in the stress modeling, event locations, and the theoretical seismicity rate model
388 it seemed inappropriate to pick such a restrictive likelihood model that rejects a model if a single
389 event is found in a region where the rate is zero. We considered resolutions such as removing data
390 points if this violation occurs. However, that would change the degrees of freedom as a function of the
391 model parameters and would render model comparison difficult to interpret. Alternatively, a non-zero
392 floor seismicity rate could be imposed (e.g. Richter et al. 2020), however, this would contradict the
393 assumptions of the model, which prefer to honor.

394 **4.4 Models with time-dependent or instantaneous stress triggering**

395 The model we have presented assumes the earthquake nucleation process is time-dependent and de-
396 scribed by a spring-slider and rate-and-state friction. However, Smith et al. (2021) explored seismicity
397 rate forecasting models, which assume that nucleation is instantaneous, dependent on a failure stress

398 distribution, and thus do not have an explicit time-dependence. Much like in this study Smith et al.
 399 (2021) observed an excellent agreement with the observed rate by using models that effectively in-
 400 corporate a threshold stress. This comparison begs the question: Does the time-dependence of friction
 401 matter when modeling the Groningen induced seismicity?

402 A possible explanation may be provided in Table 1 where it is revealed that t_a is not well deter-
 403 mined by the data. By looking at equation 1 we notice that $1/t_a$ shows up multiplying the time-integral
 404 in the denominator. The fact that t_a is not constrained implies that the integral is not important to con-
 405 strain the fit. If this integral is ignored then the model reduces to the instantaneous limit of the equation,
 406 valid at early time shortly after t_b :

$$\begin{aligned} \frac{R}{r} &= \exp\left(\frac{\Delta S(t) - \Delta S_c}{A\sigma_0}\right) && \text{if } t \geq t_b \\ \frac{R}{r} &= 0 && \text{if } t < t_b, \end{aligned} \quad (8)$$

407 which is not explicitly time-dependent much like models explored by Smith et al. (2021) and further-
 408 more takes on a similar functional form as the extreme threshold model (Bourne et al. 2018):

$$R_{ET} \propto \theta_1 \frac{d\Delta S}{dt} \exp(\theta_1 \Delta S(t) + \theta_0) \quad (9)$$

409 Where R_{ET} is the extreme threshold distribution seismicity rate and θ_0, θ_1 are statistical parameter
 410 characterizing the shape of the distribution.

411 We suggest that discriminating between the time-dependent friction model presented here and the
 412 instantaneous triggering models Smith et al. (2021) can be achieved by investigating shorter time-
 413 intervals. Groningen has seasonal fluctuations in the production rate (Bourne et al. 2014). We expect
 414 that such short-term but large amplitude fluctuations will manifest differently in the model presented
 415 here compared to the Smith et al. (2021) models. From a physical point of view; an ongoing nucleation
 416 can be modulated by the stress fluctuation. From a mathematical point of view; significant differences
 417 are expected since in the Smith et al. (2021) models the seismicity rate scales with stressing rate as in
 418 equation 9, which can become negative and thus needs imposing a non-negativity or a Kaiser effect,
 419 to avoid nonphysical effects. Such modifications necessarily introduce non-uniqueness dependent on
 420 the users' implementation. However, in the Dieterich (1994) class of models there is no explicit de-
 421 pendence of seismicity rate on the time-derivative of stress. Thus the model maintains validity even
 422 for negative stressing rates or non-differentiable stressing histories. In conclusion, we suggest that for
 423 Groningen and by investigating yearly seismicity rate that we cannot discriminate between models
 424 that assume time-dependent friction and time-independent friction.

5 CONCLUSIONS

We have presented a new Coulomb rate-and-state model (equation 1) that assumes sources can initially be well below steady state. The derivation of the model (Appendix A and B) shows that a simple stress threshold ΔS_c is needed, regardless of stressing history, to bring the seismic source above steady state. We have compared the new Threshold model to the original Dieterich (1994) model using the data from the Groningen gas field in the Netherlands. We obtain much improved agreement using the Threshold model in terms of time-series fitting to the observed seismicity rate and better agreement with the observed maximum magnitude with time. The two model provide similar agreement in terms of spatial distribution of events.

ACKNOWLEDGMENTS

E.R.H. formulated the main research questions in consultation with J-P.A. and S.J.B. E.R.H. derived the threshold model, and carried out data and model comparison. E.R.H. and J.D.S. developed code and methods for data and model comparison and visualization. J-P.A. and S.J.B helped interpret results. E.R.H wrote the manuscript with input from all authors.

E.R.H. acknowledges support from the Geophysics Option Postdoctoral Fellowship at Caltech. J.S. was supported for this project by the NSF centre of Geomechanics and Mitigation of Geohazards (GMG). We gratefully acknowledge data and support from Nederlandse Aardoli Maatschappij (Jan Van Elk, Gini Ketellar and Dirk Doornhof), Shell Global Solutions (Stijn Bierman, Steve Oates, Rick Wentinck, Xander Campman, Alexander Droujinine and Chris Harris), and Koninklijk Nederlands Meteorologisch Instituut for the open source earthquake location information. (<http://www.knmi.nl/>). We thank the IUCRC program of the National Science Foundation for support though grant 1822214 to GMG.

DATA AVAILABILITY

Data used in this paper, from which the stress model is derived, has been previously published in Smith et al. (2019). Seismic data and catalogs are provided by Koninklijk Nederlands Meteorologisch Instituut (<http://www.knmi.nl/>).

REFERENCES

Bourne, S. J. & Oates, S. J., 2017. Extreme threshold failures within a heterogeneous elastic thin sheet and the spatial-temporal development of induced seismicity within the groningen gas field, *Journal of Geophysical*

- 454 *Research: Solid Earth*, **122**(12), 10,299–10,320.
- 455 Bourne, S. J. & Oates, S. J., 2020. Stress-dependent magnitudes of induced earthquakes in the groningen gas
456 field, *Journal of Geophysical Research: Solid Earth*, **125**(11), e2020JB020013.
- 457 Bourne, S. J., Oates, S. J., van Elk, J., & Doornhof, D., 2014. A seismological model for earthquakes induced
458 by fluid extraction from a subsurface reservoir, *Journal of Geophysical Research: Solid Earth*, **119**(12), 8991–
459 9015.
- 460 Bourne, S. J., Oates, S. J., & van Elk, J., 2018. The exponential rise of induced seismicity with increasing
461 stress levels in the Groningen gas field and its implications for controlling seismic risk, *Geophysical Journal
462 International*, **213**(3), 1693–1700.
- 463 Candela, T., Osinga, S., Ampuero, J.-P., Wassing, B., Pluymaekers, M., Fokker, P. A., van Wees, J.-D., de Waal,
464 H. A., & Muntendam-Bos, A. G., 2019. Depletion-induced seismicity at the groningen gas field: Coulomb
465 rate-and-state models including differential compaction effect, *Journal of Geophysical Research: Solid Earth*,
466 **124**(7), 7081–7104.
- 467 Cattania, C., Hainzl, S., Wang, L., Roth, F., & Enescu, B., 2014. Propagation of coulomb stress uncertainties
468 in physics-based aftershock models, *Journal of Geophysical Research: Solid Earth*, **119**(10), 7846–7864.
- 469 Dempsey, D. & Riffault, J., 2019. Response of induced seismicity to injection rate reduction: Models of delay,
470 decay, quiescence, recovery, and oklahoma, *Water Resources Research*, **55**(1), 656–681.
- 471 Dempsey, D. & Suckale, J., 2017. Physics-based forecasting of induced seismicity at groningen gas field, the
472 netherlands, *Geophysical Research Letters*, **44**(15), 7773–7782.
- 473 Dieterich, J., 1994. A constitutive law for rate of earthquake production and its application to earthquake
474 clustering, *Journal of Geophysical Research: Solid Earth*, **99**(B2), 2601–2618.
- 475 Dieterich, J., Cayol, V., & Okubo, P., 2000. The use of earthquake rate changes as a stress meter at kilauea
476 volcano, *Nature*, **408**(6811), 457–460.
- 477 Dieterich, J. H., 1979. Modeling of rock friction: 1. experimental results and constitutive equations, *Journal
478 of Geophysical Research: Solid Earth*, **84**(B5), 2161–2168.
- 479 Dost, B., Ruigrok, E., & Spetzler, J., 2017. Development of seismicity and probabilistic hazard assessment for
480 the groningen gas field, *Netherlands Journal of Geosciences*, **96**(5), s235–s245.
- 481 Ellsworth, W. L., 2013. Injection-induced earthquakes, *Science*, **341**(6142).
- 482 Foreman-Mackey, D., Hogg, D. W., Lang, D., & Goodman, J., 2013. emcee: the mcmc hammer, *Publications
483 of the Astronomical Society of the Pacific*, **125**(925), 306.
- 484 Gardner, J. & Knopoff, L., 1974. Is the sequence of earthquakes in southern california, with aftershocks
485 removed, poissonian?, *Bulletin of the Seismological Society of America*, **64**(5), 1363–1367.
- 486 Goodman, J. & Weare, J., 2010. Ensemble samplers with affine invariance, *Communications in applied math-
487 ematics and computational science*, **5**(1), 65–80.
- 488 Hainzl, S., Steacy, D., & Marsan, S., 2010. Seismicity models based on Coulomb stress calculations, *Commu-
489 nity Online Resource for Statistical Seismicity Analysis*, Available at <http://www.corssa.org>.
- 490 Heimisson, E. R., 2019. Constitutive law for earthquake production based on rate-and-state friction: Theory

- 491 and application of interacting sources, *Journal of Geophysical Research: Solid Earth*, **124**(2), 1802–1821.
- 492 Heimisson, E. R. & Segall, P., 2018. Constitutive law for earthquake production based on rate-and-state
493 friction: Dieterich 1994 revisited, *Journal of Geophysical Research: Solid Earth*, **123**(5), 4141–4156.
- 494 Hogg, R. V., McKean, J., & Craig, A. T., 2019. *Introduction to mathematical statistics, Eighth Edition*, Pearson
495 Education.
- 496 Hsieh, P. A. & Bredehoeft, J. D., 1981. A reservoir analysis of the denver earthquakes: A case of induced
497 seismicity, *Journal of Geophysical Research: Solid Earth*, **86**(B2), 903–920.
- 498 Hunfeld, L. B., Niemeijer, A. R., & Spiers, C. J., 2017. Frictional properties of simulated fault gouges from
499 the seismogenic groningen gas field under in situ p–t–chemical conditions, *Journal of Geophysical Research:
500 Solid Earth*, **122**(11), 8969–8989.
- 501 Jia, K., Zhou, S., Zhuang, J., Jiang, C., Guo, Y., Gao, Z., Gao, S., Ogata, Y., & Song, X., 2020. Nonstation-
502 ary background seismicity rate and evolution of stress changes in the changing salt mining and shale-gas
503 hydraulic fracturing region, Sichuan Basin, China, *Seismological Research Letters*, **91**(4), 2170–2181.
- 504 Kolawole, F., Johnston, C., Morgan, C., Chang, J., Marfurt, K., Lockner, D., Reches, Z., & Carpenter, B., 2019.
505 The susceptibility of oklahoma’s basement to seismic reactivation, *Nature Geoscience*, **12**(10), 839–844.
- 506 Langenbruch, C. & Zoback, M. D., 2016. How will induced seismicity in oklahoma respond to decreased
507 saltwater injection rates?, *Science Advances*, **2**(11).
- 508 Linker, M. F. & Dieterich, J. H., 1992. Effects of variable normal stress on rock friction: Observations and
509 constitutive equations, *J. Geophys. Res. Solid Earth*, **97**(B4), 4923–4940.
- 510 Marone, C., 1998. Laboratory-derived friction laws and their application to seismic faulting, *Annu. Rev. Earth
511 Pl. Sc.*, **26**(1), 643–696.
- 512 Marsan, D. & Lengline, O., 2008. Extending earthquakes’ reach through cascading, *Science*, **319**(5866),
513 1076–1079.
- 514 Maurer, J., Kane, D., Nyst, M., & Velasquez, J., 2020. Risk from oklahoma’s induced earthquakes: The cost
515 of declustering, *Bulletin of the Seismological Society of America*.
- 516 Menke, W., 2018. *Geophysical data analysis: Discrete inverse theory*, Academic press.
- 517 Mizrahi, L., Nandan, S., & Wiemer, S., 2021. The Effect of Declustering on the Size Distribution of Main-
518 shocks, *Seismological Research Letters*.
- 519 Nederlandse Aardolie Maatschappij, 2013. A technical addendum to the winningsplan groningen 2013 subsi-
520 dence, induced earthquakes and seismic hazard analysis in the groningen field, *NAM, Assen*.
- 521 Norbeck, J. H. & Rubinstein, J. L., 2018. Hydromechanical earthquake nucleation model forecasts onset,
522 peak, and falling rates of induced seismicity in oklahoma and kansas, *Geophysical Research Letters*, **45**(7),
523 2963–2975.
- 524 Ogata, Y., 1998. Space-time point-process models for earthquake occurrences, *Annals of the Institute of Sta-
525 tistical Mathematics*, **50**(2), 379–402.
- 526 Post, R. A., Michels, M. A., Ampuero, J.-P., Candela, T., Fokker, P. A., van Wees, J.-D., van der Hofstad,
527 R. W., & van den Heuvel, E. R., 2021. Interevent-time distribution and aftershock frequency in non-stationary

- 528 induced seismicity, *Scientific reports*, **11**(1), 1–10.
- 529 Raleigh, C. B., Healy, J. H., & Bredehoeft, J. D., 1976. An experiment in earthquake control at rangely,
530 colorado, **191**(4233), 1230–1237.
- 531 Richter, G., Hainzl, S., Dahm, T., & Zöller, G., 2020. Stress-based, statistical modeling of the induced seis-
532 micity at the groningen gas field, the netherlands, *Environmental Earth Sciences*, **79**, 1–15.
- 533 Ruina, A., 1983. Slip instability and state variable friction laws, *Journal of Geophysical Research: Solid Earth*,
534 **88**(B12), 10359–10370.
- 535 Smith, J. D., Avouac, J.-P., White, R. S., Copley, A., Gualandi, A., & Bourne, S., 2019. Reconciling the long-
536 term relationship between reservoir pore pressure depletion and compaction in the groningen region, *Journal*
537 *of Geophysical Research: Solid Earth*, **124**(6), 6165–6178.
- 538 Smith, J. D., White, R. S., Avouac, J.-P., & Bourne, S., 2020. Probabilistic earthquake locations of induced
539 seismicity in the groningen region, the netherlands, *Geophysical Journal International*, **222**(1), 507–516.
- 540 Smith, J. D., Heimisson, E. R., Bourne, S. J., & Avouac, J.-P., 2021. Stress-based forecasting of induced seis-
541 micity with instantaneous earthquake failure functions: Applications to the groningen gas reservoir., *Earth-*
542 *ArXiv*.
- 543 Stein, R. S., 1999. The role of stress transfer in earthquake occurrence, *Nature*, **402**(6762), 605–609.
- 544 Van der Elst, N. J., Page, M. T., Weiser, D. A., Goebel, T. H., & Hosseini, S. M., 2016. Induced earthquake
545 magnitudes are as large as (statistically) expected, *Journal of Geophysical Research: Solid Earth*, **121**(6),
546 4575–4590.
- 547 Willacy, C., van Dedem, E., Minisini, S., Li, J., Blokland, J.-W., Das, I., & Droujinine, A., 2019. Full-waveform
548 event location and moment tensor inversion for induced seismicity, *Geophysics*, **84**(2), KS39–KS57.
- 549 Zhai, G., Shirzaei, M., Manga, M., & Chen, X., 2019. Pore-pressure diffusion, enhanced by poroelastic
550 stresses, controls induced seismicity in oklahoma, *Proceedings of the National Academy of Sciences*, **116**(33),
551 16228–16233.

552 APPENDIX A: TIME TO ACTIVATION: SINGLE SOURCE

553 We start by describing a single seismic source, idealized as a spring and slider system and investigate
554 the state evaluation equation (Dieterich 1979; Ruina 1983),

$$\dot{\theta} = 1 - \frac{\delta\theta}{d_c} = 1 - \Omega \quad (\text{A.1})$$

555 If $\Omega \gg 1$, the source is accelerating towards instability (active and well above steady state), if
556 $\Omega \ll 1$ the source is in healing phase (inactive and well below steady state). If $\Omega = 1$ the source is at
557 steady state ($\dot{\theta} = 0$). We start by assuming that the seismic source is at time $t = 0$ well below steady
558 state. We shall refer to a seismic source that is well below steady state as inactive. Here we shall see

559 that if all seismic sources in a population are inactive there will be no seismicity produced until we
560 reach a certain stress where they become active.

561 Assuming $\Omega \ll 1$, then

$$\theta = \theta_0 + t. \quad (\text{A.2})$$

562 The rate-and-state friction law and force balance becomes (following notations of Heimisson &
563 Segall (2018))

$$\tau(t) - k\delta(t) = \sigma(t) \left(\mu + A \log \frac{\dot{\delta}(t)}{V^*} + B \log \frac{(\theta_0 + t)V^*}{d_c} \right) \quad (\text{A.3})$$

564 Rearranging provides:

$$K(t) \left(\frac{\theta_0}{\theta_0 + t} \right)^{(B/A)} = \frac{\dot{\delta}}{\dot{\delta}_0} \exp \left(\frac{k\delta}{A\sigma(t)} \right) \quad (\text{A.4})$$

565 Where

$$K(t) = \exp \left(\frac{\tau(t)}{A\sigma(t)} - \frac{\tau_0}{A\sigma_0} \right) \approx \exp \left(\frac{\Delta S(t)}{A\sigma_0} \right) \quad (\text{A.5})$$

566 where the approximation is the Coulomb stress approximation discussed in detail by Heimisson &
567 Segall (2018). The initial slip speed can be found from equation A.3, by introducing the initial values
568 for all field: $\dot{\delta}_0 = V^* \exp(\tau_0/A\sigma_0 - \mu/A)(V^*\theta_0/d_c)^{-B/A}$. We have introduced the initial slip speed
569 into equation A.4 for compactness and clarity. In other words, $\Delta S(t) = \tau(t) - \mu\sigma(t)$ represents
570 modified Coulomb stress, with $\mu = \tau_0/\sigma_0 - \alpha$. τ_0 and σ_0 are the initial background shear and effective
571 normal stress respectively, α is the Linker-Dieterich constant (Linker & Dieterich 1992).

572 If a seismic source is well below steady state it will slip a very small distance until it will be
573 perturbed sufficiently to go above steady state. We thus assume in Eq. A.4 that $k\delta/A\sigma_0 \ll 1$ and thus:

$$\frac{\dot{\delta}}{\dot{\delta}_0} = K(t) \left(\frac{\theta_0}{\theta_0 + t} \right)^{(B/A)} \quad (\text{A.6})$$

574 If the seismic sources have been healing for much longer time than they are perturbed then $\theta_0 \gg t$.
575 This is likely always true for seismically inactive faults that have been healing for geological time-
576 scales, but are perturbed on the time scale of months to years. But we emphasize that the threshold
577 model requires that the time-scale of the stress perturbations is short compared to the time-scale over
578 which healing occurs. Thus:

$$\frac{\dot{\delta}}{\dot{\delta}_0} = K(t) \quad (\text{A.7})$$

579 Now let us assume that a source activates at $\Omega_c \gtrsim 1$, but $\Omega_c = 1$ is exactly steady-state. Then we
580 find a critical stress perturbation ΔS_c (using the Coulomb stress approximation).

$$\frac{\Delta S_c}{A\sigma_0} = \log\left(\frac{\Omega_c}{\Omega_0}\right) \quad (\text{A.8})$$

581 By virtue of the slow growth of the logarithm we may infer from equation A.8 that perturbations
582 of the order of $A\sigma_0$ are universally needed to activate the population. Once the threshold is achieved
583 the assumption of well above steady state is justified and the Dieterich theory can be applied. Then the
584 time t_b at which the seismic source is activated is the solution of the following equation:

$$\Delta S(t = t_b) = \Delta S_c = A\sigma_0 \log\left(\frac{\Omega_c}{\Omega_0}\right), \quad (\text{A.9})$$

585 where we infer that the critical stress ΔS_c will typically be in the range of 1 – 10 $A\sigma_0$. In practical ap-
586 plications either ΔS_c or t_b needs to be determined. This estimations may be done through an inversion
587 process, but it is worth noting that typically t_b can considered an observable, at least up to reasonable
588 certainty. It would then represent the time since injection, extraction, or other perturbations started
589 until the time that seismic activity begins. However, If the stress perturbation in space is heteroge-
590 neous then t_b will also likely vary in space. Through a stress model and an estimation of $A\sigma_0$ one can
591 relate t_b to ΔS_c , which may not vary strongly in space due to logarithmic dependence on Ω_c/Ω_0 and
592 could potentially have a predictive value for the onset of seismicity in other regions. It may, therefore,
593 be more straightforward to directly invert for ΔS_c , assuming that it is spatially uniform, instead of
594 estimating t_b .

595 APPENDIX B: NEW CONSTITUTIVE LAW: A THRESHOLD MODEL

596 In the previous section we derived a stress threshold ΔS_c at which a seismic source can be considered
597 active or above steady state. Now we assume that once we reach ΔS_c the whole population of seismic
598 sources is moved above steady state, in other word, all sources become active. This assumptions is
599 likely reasonable as long as the variability of ΔS_c in the populations of seismic sources is less than
600 $A\sigma_0$. Further, for the sake of mathematical tractability, we assume the sources cannot be moved below
601 steady state once it is well above steady state or activated.

By assuming that the seismic sources under arbitrary stressing conditions are activated at time
 $t = t_b$ and for background conditions at t_b^0 then equation 17 in Heimisson & Segall (2018) can be

rewritten in the following manner:

$$\int_{t_b}^t K(t') dt' = \int_{t_b^o}^{t_b^o + N/r} e^{t'/t_a} dt', \quad (\text{B.1})$$

602 where t_b is a constant and represents the time when $\Delta S(t = t_b) = A\sigma_0 \log(\frac{\Omega_c}{\Omega_0})$, $t_b^o = t_a \log(\frac{\Omega_c}{\Omega_0}) =$
 603 $t_a \Delta S_c / (A\sigma_0)$. Thus implementing the Coulomb stress approximation, which will be used to replace
 604 $K(t)$ hereafter, we find:

$$\int_{t_b}^t \exp\left(\frac{\Delta S(t')}{A\sigma_0}\right) dt' = t_a \frac{\Omega_c}{\Omega_0} \left(e^{N/rt_a} - 1\right). \quad (\text{B.2})$$

605 Solving for N gives

$$\frac{N}{r} = t_a \log\left(\frac{1}{t_a \frac{\Omega_c}{\Omega_0}} \int_{t_b}^t \exp\left(\frac{\Delta S(t')}{A\sigma_0}\right) dt' + 1\right), \quad (\text{B.3})$$

606 or alternatively

$$\frac{N}{r} = t_a \log\left(\frac{1}{t_a} \int_{t_b}^t \exp\left(\frac{\Delta S(t') - \Delta S_c}{A\sigma_0}\right) dt' + 1\right), \quad (\text{B.4})$$

607 Comparison to equation 18 in Heimisson & Segall (2018) and equation B.4 B.4 reveals that the
 608 theory proposed here reduced to the Dieterich (1994) theory in the limit when the threshold stress
 609 $\Delta S_c = 0$, as should be expected. Were we note that $N = 0$ if $t < t_b$. Seismicity rate R is found by
 610 differentiation:

$$\frac{R}{r} = \frac{K(t)}{\left(\frac{1}{t_a} \int_{t_b}^t K(t') dt' + \frac{\Omega_c}{\Omega_0}\right)} \quad (\text{B.5})$$

611 or alternatively

$$\frac{R}{r} = \frac{\exp\left(\frac{\Delta S(t) - \Delta S_c}{A\sigma_0}\right)}{\frac{1}{t_a} \int_{t_b}^t \exp\left(\frac{\Delta S(t') - \Delta S_c}{A\sigma_0}\right) dt' + 1}, \quad (\text{B.6})$$

612 which is equation 1 in the maintext.

613 **APPENDIX C: DERIVATION OF SEISMICITY-RATE VARIANCE**

614 Here we derive the simple variance model that is used in the study to characterize the uncertainty in
 615 the binned seismicity rate.

616 First we note the Poissonian probability distribution

$$P(X = x_i) = \frac{e^{-\lambda} \lambda^{x_i}}{x_i!}, \quad (\text{C.1})$$

617 where λ is the expected value of X , which we interpret in this study as the number of events in some
618 time-interval, and also the variance of X .

The distribution of n samples from the distribution is also a Poisson distribution of random variable $Y = \sum_{i=1}^n x_i$ with the expected value of $n\lambda$ (e.g. Hogg et al. 2019, theorem 3.2.1) thus

$$P(Y = \sum_{i=1}^n x_i) = \frac{e^{-n\lambda} (n\lambda)^{\sum_{i=1}^n x_i}}{(\sum_{i=1}^n x_i)!}. \quad (\text{C.2})$$

where $\sum_{i=1}^n x_i = 0, 1, 2, \dots$. The distribution of the sample mean \bar{X} can be obtained by substitution $\sum_{i=1}^n x_i = n\bar{X}$

$$P(\bar{X} = \bar{x}) = \frac{e^{-n\lambda} (n\lambda)^{n\bar{x}}}{(n\bar{x})!}, \quad (\text{C.3})$$

619 where $\bar{x} \in \{0, 1/n, 2/n, \dots\}$ or alternatively $\bar{x} = j/n$, where $j \in \{0, 1, 2, \dots\}$. We can thus
620 compute the expected value of the sample mean distribution:

$$\langle \bar{X} \rangle = \sum_{j=0}^{\infty} \frac{j}{n} \frac{e^{-n\lambda} (n\lambda)^j}{j!} = \lambda. \quad (\text{C.4})$$

621 This is not unexpected since the mean of the sample mean distribution must also be the mean of the
622 distribution that is being sampled. However, the same is not true for the variance.

$$\text{Var}(\bar{X}) = \sum_{j=0}^{\infty} \left(\frac{j}{n} - \lambda \right)^2 \frac{e^{-n\lambda} (n\lambda)^j}{j!} = \frac{\lambda}{n}. \quad (\text{C.5})$$

623 The variance of the sample mean represents the number of events observed in a particular bin and
624 we will also call n as we keep in mind that the observed number of events is the same number as
625 the number of samples. Thus we see that the variance is reduced the more samples are available as is
626 expected.

627 In our case we estimate the characteristic rate R as the number of events n divided by the bin
628 length, or $R = N/\Delta t$. Thus the variance of the rate is $\text{Var}(R) = \text{Var}(\bar{X})/\Delta t^2 = \lambda/(n\Delta t^2)$. Equation
629 C.4 shows that we can approximate $\lambda \approx n$. We then finally find $\text{Var}(R) = 1/\Delta t^2$ and the standard
630 deviation thus $1/\Delta t$. In this study we have picked $\Delta t = 1$ year, and thus the estimate of the variance
631 is simply 1.